Structural Vibration-Based Classification and Prediction of Delamination in Smart Composite Laminates using Deep Learning Neural Network

Asif Khan[1], Dae-Kwan Ko[1], Soo Chul Lim[1*] and Heung Soo Kim[1*]

[1]Department of Mechanical, Robotics and Energy Engineering, Dongguk University-Seoul, 30 Pil-dong 1 Gil, Jung-gu, Seoul, 04620, Republic of Korea

* Corresponding authors: heungsoo@dgu.edu; Tel: +82-2-2260-8577, Fax: +82-2-2263-9379

limsc@dgu.edu; Tel: +82-2-2260-3823, Fax: +82-2-2263-9379

Abstract

This paper proposes a Convolutional Neural Network (CNN) based approach for the classification and prediction of various types of in-plane and through-the-thickness delamination in smart composite laminates using low-frequency structural vibration outputs. An electromechanically coupled mathematical model is developed for the healthy and delaminated smart composite laminates, and their structural vibration responses are obtained in the time domain. Short Time Fourier Transform (STFT) is employed to transform the transient responses into two-dimensional spectral frame representation. A convolutional neural network is incorporated to distinguish between the damaged and undamaged states, as well as various types of damage of the laminated composites, by automatically extracting discriminative features from the vibration-based spectrograms. The CNN showed a classification accuracy of 90.1 % on one healthy and 12 delaminated cases. The study of the confusion matrix of CNN provided further insights into the physics of the problem. The predictive performance of a pre-trained CNN classifier was also evaluated on unseen cases of delamination, and physically consistent results were obtained.

Keywords: A. Smart materials, B. Delamination, B. Vibration, D. Non-destructive testing

1. Introduction

Laminated composites are characterized by the advantageous properties of high specific strength, high specific stiffness, design flexibility, good damping capacity, and high fatigue life, compared to metals. These materials are becoming preferred materials in a variety of industries, such as aerospace, aeronautics, naval, and automotive [1-6], among others. However, owing to their orthotropic nature, laminated composites are vulnerable to various complex and inconspicuous modes of failure, such as matrix crack, fiber breakage, and delamination [7-10], either during service life, or the manufacturing process. Delamination is a major and frequently occurring failure mode that tremendously affects the strength, stiffness, stability, and usable service life of laminated composites, and may eventually lead to catastrophic failure of the composite structures [11-13]. Hence, the detection, quantification, and localization of delamination in composite laminates are critical for the safe and reliable implementation of these materials in various real world applications.

In the literature, a vast range of techniques have been proposed for the detection, quantification, and localization of delamination in laminated composites, among which vibration-based methods have been proven to be more adequate [14, 15]. In general, the vibration-based method can be divided into two categories: low-frequency

structural vibration-based methods, and high-frequency guided waves based methods. The common attributes in the former for delamination assessment are modal parameters, such as natural frequency, modal damping, mode shapes and mode shape curvatures, frequency response function (FRF), wavelet coefficients, auto-regressive parameters, and power spectral density (PSD) of the transient responses [16-22], whereas the common discriminative features for the pristine and delaminated laminates in the latter are correlation coefficients, phase change, the difference of amplitudes, the difference of the time of occurrence of fundamental modes, frequency centroids, and wavelet energy [23-25]. In general, low-frequency structural vibration responses (i.e., the vibratory behavior in the fundamental modes) capture the global behavior (i.e., presence of damage) of the structure, whereas the vibration responses at higher-frequencies capture the local responses (i.e., location of damage) of the structures [26]. Hence, in the published literature, structural vibration-based methods have been employed for the global assessment of delamination [16], whereas guided waves-based methods have been used for the local assessment of damage in laminated composites [27, 28]. However, the guided waves-based methods suffer from the disadvantages of being active in nature; i.e., these methods require a voltage supply and function generating signal, and the requirement of data acquisition at high rate to gain useful signal resolution [29].

In actual practice, structural vibration response obtained through smart material (e.g., piezoelectrics and electroactive polymers) is more readily available for the assessment of damage in composite structures. However, as mentioned earlier, most of the attributes of structural vibration (e.g., natural frequency, modal damping, FRF etc.) are global parameters, and cannot be used for the localization of damage in laminated composites [30]. In this work, an output-based data-driven technique is proposed for the global and local assessment of delamination in smart composite laminates from their low-frequency structural vibration response. Experimentally verified improved layerwise theory [31], higher order electric potential field [32], and the finite element method are employed to develop an electromechanically coupled dynamic model for the pristine and delaminated smart composite structures. Transient responses of the healthy and delaminated composites are obtained via a piezoelectric sensor by solving the dynamic model in the time domain. The transient histories are transformed into spectrograms via discrete Fast Fourier Transform (FFT) and a sliding window technique. The structural vibration-based spectrograms are employed for the training, cross-validation, and testing of convolutional neural network (CNN). The confusion matrix of CNN showed physically consistent results, and an overall classification accuracy of 90.1 % is obtained.

The essence of the proposed technique is that it requires only low-frequency structural vibration responses for the detection and localization of delamination in smart composite laminates.

The rest of the paper is organized as follows: section 2 describes the development of the electromechanically coupled dynamic mathematical model for the pristine and delaminated smart composite structures. Section 3 describes the numerical implementation of the mathematical model on a 16-layers cross-ply laminated composite plate with surface bonded piezoelectric sensor and actuator. Random vibration responses of the intact and delaminated smart composite laminates are obtained and discussed in both the time and frequency domains. Section 4 outlines the proposed methodology for the global and local assessment of delaminations from structural vibration. Section 5, which includes the contribution of the current work, concludes the paper.

2. Mathematical Modeling

This section describes the development of an electromechanically coupled dynamic mathematical model for the pristine and delaminated smart composite laminates. The displacement and electric potential fields are modelled on the basis of improved layerwise theory [33] and higher-order electric potential field [32], respectively. The two fields are implemented via finite element method, and variational principles are employed to derive the governing equation of motion.

2.1 Displacement Field with Delaminations

According to improved layerwise theory [31, 33], for an N-layered laminated composite, the displacement of a point with coordinates (*x, y, z*) is described by the superposition of first-order shear deformation theory and layerwise functions, as shown by Eq. (1)

$$U_1^k(x,y,z,t) = u_1 + A_1^k(z)\phi_1 + B_1^k(z)\phi_2 + C_1^k(z)w_{,x} + D_1^k(z)w_{,y} + \bar{E}_1^j(z)\bar{w}_{,x}^j + \bar{F}_1^j(z)\bar{w}_{,y}^j + \sum_{j=1}^{N-1}\bar{u}_1^j H(z-z_j)$$

$$U_2^k(x,y,z,t) = u_2 + A_2^k(z)\phi_1 + B_2^k(z)\phi_2 + C_2^k(z)w_{,x} + D_2^k(z)w_{,y} + \bar{E}_2^j(z)\bar{w}_{,x}^j + \bar{F}_2^j(z)\bar{w}_{,y}^j + \sum_{j=1}^{N-1}\bar{u}_2^j H(z-z_j)$$

$$U_3^k(x,y,z,t) = w(x,y,t) + \sum_{j=1}^{N-1}\bar{w}^j(x,y,t)H(z-z_j) \qquad (1)$$

where, U_1^k and U_2^k are the in-plane displacements, and U_3^k is the transverse deflection of the *k*th layer of the laminate. The terms u_1, u_2 and w refer to the displacements of mid-plane along the *x*, *y*, and *z*-axis, respectively. The quantities ϕ_1 and ϕ_2 denote the rotation of normal to the mid-plane about the *x* and *y* axis, respectively. The terms

$\bar{u}_1^j$, $\bar{u}_2^j$ and $\bar{w}^j$, along with the Heaviside unit step function *H*, address the discontinuity of the displacement field by quantitatively accounting for the sliding of the in-plane displacements, and possible jump of the out-of-plane displacement at the delaminated interfaces. The index *j* refers to the delaminated interface: e.g., z_j denotes the delaminated interface, and $\bar{u}_1^j$ refers to the in-plane sliding along the *x*-axis at the *j*th debonded interface. The terms $A_i^k(z)$, $B_i^k(z)$, $C_i^k(z)$, $D_i^k(z)$, $\bar{E}_i^k(z)$, and $\bar{F}_i^k(z)$ (i =*1, 2*) are layerwise functions that are expressed in terms of the material and geometric properties of the *N*-layered laminate through *4N* constraint equations of displacement and shear stress continuity conditions [33].

2.2 Electric Potential Field

To satisfy the surface boundary conditions of the applied voltages and the charge conservation law, a cubic distribution of the electric potential filed along the thickness of piezoelectric patches is assumed [32]. The resulting higher-order potential field for the *q*th piezoelectric layer is given by Eq. (2):

$$\phi^q(x,y,z,t) = \phi_0^q(x,y,t) - \left(z - z_0^q\right)E_z^q(x,y,t) + 4\left(\frac{z - z_0^q}{h^q}\right)^2 \times\left[\left(z - z_0^q\right)\left(\frac{\bar{\phi}^q(x,y,t)}{h^q} + E_z^q(x,y,t)\right) - \phi_0^q(x,y,t)\right] \tag{2}$$

where, ϕ_0^q and E_z^q denote the electric potential and electric field at the mid-plane of the *q*th piezoelectric patch, respectively. The terms z_0^q and h^q denote the mid-plane position and thickness of the piezoelectric transducer, respectively. The quantity $\bar{\phi}^q$ refers to the potential difference between the top and bottom electrodes of piezoelectric patches.

2.3 Finite element implementation

From Eq. (1), the displacement field of a healthy laminated composite with *N*-layers can be expressed in terms of the variables u_1, u_2, w, $w_{,x}$, $w_{,y}$, ϕ_1, and ϕ_2, whereas the displacement field of a delaminated composite can be expressed in terms of the variables u_1, u_2, w, $w_{,x}$, $w_{,y}$, ϕ_1, ϕ_2, $\bar{u}_1^j$, $\bar{u}_2^j$, $\bar{w}^j$, $\bar{w}_{,x}^j$, and $\bar{w}_{,y}^j$. On the other hand, the higher-order electric potential field of piezoelectric patches can be expressed in terms of the variables ϕ_0^q and E_z^q.

The two fields of Eqs. (1) and (2) are implemented via finite element method for a four-node plate element. The in-plane structural unknowns (u_1, u_2, ϕ_1, ϕ_2, $\bar{u}_1^j$, $\bar{u}_2^j$) and electrical unknowns (ϕ_0^q, E_z^q) are interpolated via linear Lagrange interpolation function (N_m), whereas the out-of-plane structural unknowns (w, $\bar{w}^j$) are interpolated

via Hermite cubic interpolation function (H_m, H_{xm}, H_{ym}). In this way, the structural and electrical unknowns can be expressed in terms of nodal values and interpolation functions, as given by Eq. (3):

$$\begin{aligned}
&\left(u_1, u_2, \phi_1, \phi_2, \bar{u}_1^j, \bar{u}_2^j\right) = \sum_{m=1}^{4} N_m \left[\left(u_1\right)_m, \left(u_2\right)_m, \left(\phi_1\right)_m, \left(\phi_2\right)_m, \left(\bar{u}_1^j\right)_m, \left(\bar{u}_2^j\right)_m\right] \\
&w = \sum_{m=1}^{4} \left[H_m \left(w\right)_m + H_{xm} \left(w_{,x}\right)_m + H_{ym} \left(w_{,y}\right)_m\right] \\
&\bar{w}^j = \sum_{m=1}^{4} \left[H_m \left(\bar{w}\right)_m + H_{xm} \left(\bar{w}_{,x}\right)_m + H_{ym} \left(\bar{w}_{,y}\right)_m\right] \\
&\left(\phi_0^q, E_z^q\right) = \sum_{m=1}^{4} \left[N_m \left(\phi_0^q\right)_m, N_m \left(E_z^q\right)_m\right]
\end{aligned} \tag{3}$$

2. 4 Equation of motion

The finite element based governing equation of motion can be derived using the variational principles, as follows:

$$\delta\pi_u = -\int_0^{t_0}\int_V \left(\rho \ddot{u}_i \delta u_i + \gamma \dot{u}_i \delta u_i + \sigma_{ij} \delta\varepsilon_{ij}\right) dV dt + \int_0^{t_0}\int_S t_i \delta u_i \, dS dt = 0$$

$$\delta\pi_u = -\int_0^{t_0}\int_V D_i \, \delta\phi_{,i} \, dV dt + \int_0^{t_0}\int_S q_e \delta\phi \, dS \, dt = 0 \tag{4}$$

where, π_u and π_ϕ are the energy functional of the mechanical and electrical fields, respectively. The term ρ denotes the mass density, and γ refers to the material damping constant. The quantities t_i and q_e denote the components of the traction vector and charge density, respectively.

Substituting Eq. (3) into Eq. (4), the Equations of motion are obtained as shown by Eq. (5) in matrix form:

$$\begin{bmatrix} M_{uu} & 0 \\ 0 & 0 \end{bmatrix} \begin{Bmatrix} \ddot{d}_u \\ 0 \end{Bmatrix} + \begin{bmatrix} C_{uu} & 0 \\ 0 & 0 \end{bmatrix} \begin{Bmatrix} \dot{d}_u \\ 0 \end{Bmatrix} + \begin{bmatrix} K_{uu} & K_{u\phi} \\ K_{\phi u} & K_{\phi\phi} \end{bmatrix} \begin{Bmatrix} d_u \\ d_\phi \end{Bmatrix} = \begin{Bmatrix} F_u \\ F_\phi \end{Bmatrix} \tag{5}$$

where, d_u and d_ϕ denote the displacement and electrical unknowns, respectively. The terms M_{uu}, C_{uu}, and K_{uu} represent the mass, damping, and stiffness matrices of the smart structure, respectively. The quantities $K_{\phi u}$ and $K_{u\phi}$ denote the electromechanical coupling stiffness matrices.

3. Dynamic Analysis of Smart Composite Laminates with Delaminations

The electromechanically coupled dynamic model of section 2 is numerically implemented on a 16-layer cross-ply ($[0/90]_{4s}$) laminated composite plate with surface-bonded piezoelectric sensor and actuator, as shown in Fig. 1. The material properties of a single lamina of the host laminate are: E1=372 GPa, E2=E3=4.12 GPa,

G12=G13=3.99 GPa, G23=3.6 GPa, ρ = 1,788.5 kg/m^3, ν12 = ν13 = 0.275, ν13 = 0.42; whereas, the material properties of the isotropic piezoelectric patches (PZT-5H) are: E = 69 GPa, b11 = 14.41 nf/m, d31=d32 = 179 ×10^{-12} m/V, ρ = 7700 kg/m^3, ν = 0.31 [34].

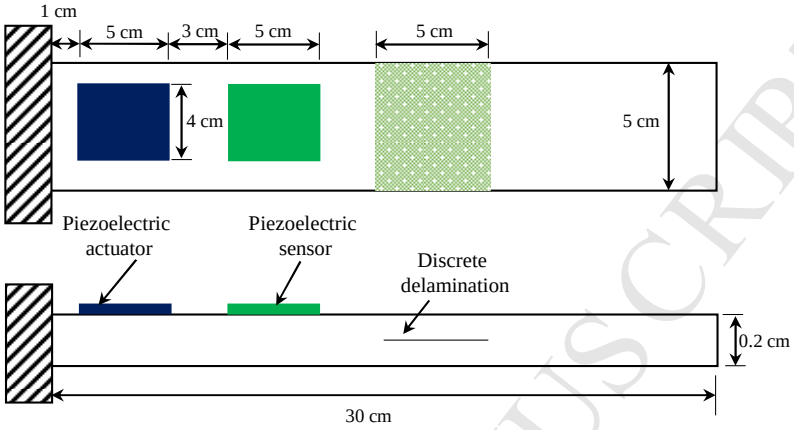

Figure 1. Physical configuration of cantilever smart laminated composite plate for numerical implementation.

Discrete delaminations of 5 cm are seeded at three different locations along the length of the plate, where each case of in-plane delamination can occur at four different interfaces along the thickness, as shown in Fig. 2:

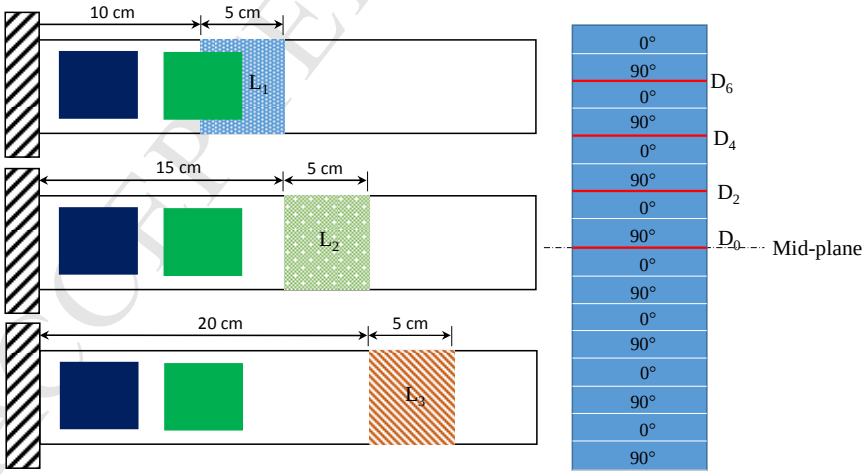

Figure 2. Geometric configuration of the smart composite plate with various discrete delaminations along the in-plane direction (**left**), and through-the-thickness direction (**right**)

In Fig. 2, D_0, D_2, D_4, and D_6 denote the presence of delamination at the mid-plane, second, fourth, and sixth interfaces from the mid-plane, respectively. The three in-plane delaminations combined with four options of through-the-thickness delaminated interfaces resulted in 12 classes of delaminations. For example, class 1 refers to the delamination at location L_1 and interface D_0 (i.e., L_1D_0); similarly, class 5 represents delamination at location L_2 and interface D_2 (L_2D_2), and so on. The smart composite laminate with perfectly bonded layers case is referred to as the healthy case (H). It should be noted that the presence of delamination at the mid-plane interface and near the clamped region is more pronounced and easily detectable than those that occur away from mid-plane interface and the clamped end of the smart composite plate [31]. Hence, different classes of delamination can be ordered as follows in terms of their detectability: L_1D_0> L_1D_2> L_1D_4> L_1D_6, L_2D_0> L_2D_2> L_2D_4> L_2D_6, L_3D_0> L_3D_2> L_3D_4> L_3D_6 and L_1D_0> L_2D_0> L_3D_0, and so on.

In real life applications, engineering structures are subjected to random input excitations from unknown sources. To simulate the actual scenario, the pristine and 12 delaminated cases of the smart composite laminates are subjected to 1,000 random harmonic excitations. The random harmonic excitations are applied in the form of voltages through the piezoelectric actuator, and the corresponding responses are measured in the form of voltage signals through the piezoelectric sensor. The transient responses are obtained by solving the electromechanically coupled equation of motion (Eq. (5)) in the time domain via Newmark's time integration algorithm [34]. For the 13 cases (i.e., healthy and 12 delaminated cases), we obtained a data set of size 13,000×1,001, where 13,000 refers to the responses of the 13 cases (1,000 responses in each case), and 1,001 represents the data points in 0.1 second of the transient response. Figure 3a compares the response signals of the healthy laminate to the first 5 random inputs, whereas Fig. 3b shows the transient responses of the healthy and delaminated cases (i.e., L_2D_0, L_2D_2, L_2D_4, L_2D_6) to the first random input.

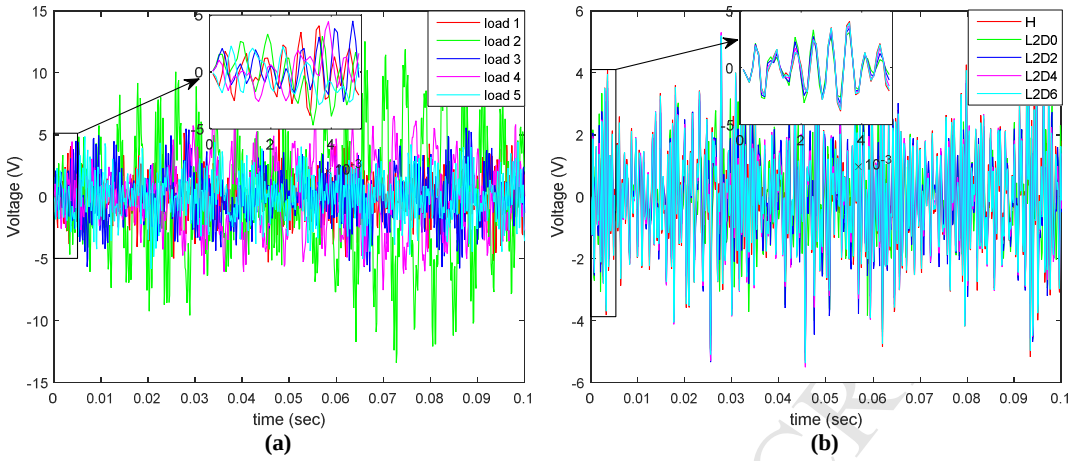

Figure 3. (a) Response signals of the healthy laminate (H) to the first 5 random inputs, (b) response signals of the Healthy, L_2D_0, L_2D_2, L_2D_4, and L_2D_6 to the first random input

Figure 4a compares the absolute values of the Fast Fourier transform (FFT) of the random responses of Fig. 3a, while Fig. 4b shows the absolute values of the FFT of the transient responses in Fig. 3b.

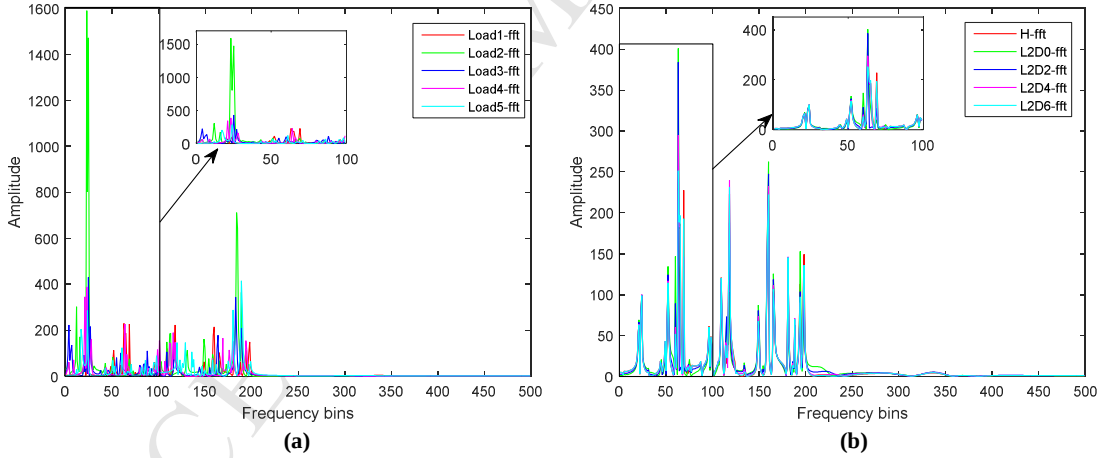

Figure 4. (a) Absolute values of the FFT of the first 5 random responses of the healthy case, (b) absolute values of the FFT of response signals of the Healthy, L_2D_0, L_2D_2, L_2D_4, and L_2D_6 to the first random input.

Figures 3a and 4a reveal that the response signals of a single case (e.g., H in this case) are distinct from each other in the time and frequency domains, respectively. Whereas, the response signals of different cases to similar inputs in Figs. 3b and 4b are hardly indistinguishable in both the time and frequency domains, respectively. To investigate the distinguishability of the transient responses of the healthy and delaminated cases, the entire data set (13,000×1,001)

is processed via conventional supervised machine learning algorithms (SVM, J48 decision tree, Random Forest, Naïve Bayes, k-nearest neighbors (KNN)), and deep learning algorithms of recurrent neural network (RNN). Table 1 compares the classification accuracy of the conventional machine learning algorithms and RNN in classifying the transient histories of the healthy and delaminated smart composite laminates into different classes.

Table 1. Comparisons of the performance of supervised learning algorithms in classifying the transient histories directly.

Classifier	**Cubic SVM**	**Medium Gaussian SVM**	**J48 Decision Tree**	**Random Forest**	**Naïve Bayes**	**K-Nearest Neighbors**	**Recurrent Neural Network**
Classification Accuracy	16.00 %	19.60 %	13.04 %	4.23 %	17.43 %	10.50 %	66.00 %

It should be noted that the purpose of using conventional machine learning is to confirm the resemblance of transient histories from damaged and undamaged cases, and should not be confused with the fact that conventional machine learning algorithms show better performance on the discriminative features extracted from the transient histories. In this work, discriminative features are extracted automatically in the section on proposed methodology.

Figures 3 and 4 and Table 1 show that the variance within the transient responses of a single case is high, while the variance within the responses of different cases (i.e., damaged, undamaged, and different cases of damages) is low. Although RNN has shown a classification accuracy of 66 %, the chances of false predictions with this accuracy will be high. Also, according to Worden et al. [35], 'without intelligent feature extraction, the more sensitive a measurement is to damage, the more sensitive it is to changing operational and environmental conditions'. Therefore, in the next section, a convolutional neural network (CNN) based methodology is proposed to deal with the current problem.

4. Delamination detection and localization by deep learning

One of the major advantages of deep learning is the autonomous extraction of discriminative features from the raw data [36]. Deep learning has been employed for the damage assessment of laminated composites [37], aircraft engines and power transformers [38], rolling element bearings [39], and the structural health monitoring of civil infrastructures [40]. The discussions in sections 1 and 3 show that the detection, quantification, and localization of delaminations in smart composite laminates from their structural vibration responses have difficulties that are

inherited from the dependency of the acquired transient histories on the operating conditions, and the fact that the vibratory responses in the fundamental modes capture the global behavior of the structure. In this section, a CNN-based methodology is proposed to address the current problem of detection and localization of delamination from low-frequency structural vibration response.

4.1 Convolutional Neural Network

The convolution neural network (CNN), a neural network structure developed for image processing, has proven to be a very efficient and effective structure for image recognition and classification [36, 41]. The network takes advantage of the fact that the input consists of images, and constrains the architecture in a more sensible way. Unlike the regular neural network, the layers of CNN are organized in 3 dimensions (width, height, and depth). In a typical CNN, four main operations: 1) Convolution, 2) Non Linearity (ReLU), 3) Pooling or Sub Sampling, and 4) Classification, are carried out in three layers: Convolutional layer, Pooling layer, and Fully-Connected layer. The primary purpose of the convolution is to extract features from the input image by sliding a filter or kernel over small patches of the image. The convolution operation is followed by a non-linear operation, such as Rectified Linear Unit (ReLU), to introduce non-linearity in CNN, as most of the real world data that is used for the learning of CNN is non-linear. Pooling or Subsampling is employed to reduce the dimensionality of the feature map obtained in the convolution operation. The convolutional and pooling layers transform the input image into a high-level feature map that is employed by the Fully-Connected layer (output layer) for the classification of the input image [42]. Full convolutional neural network architectures are formed by stacking the Convolutional, Pooling, and Fully-connected layers together. The mathematical details of each layer of CNN can be referred to in Ref. [43].

There are three key steps in the proposed approach for the classification of delamination: 1) construction of vibration-based spectrograms, 2) autonomous features extraction and classification via convolutional neural network, and 3) prediction of labels for new cases of delaminations. Section 4.2 discusses the construction of vibration-based spectrograms for input to CNN, section 4.3 focuses on network architecture, section 4.4 presents the classification of delaminations from the proposed network architecture, and section 4.5 discusses the prediction of labels for new cases of delaminations.

4.2 Vibration Spectrograms

The transient responses of the healthy and delaminated smart composite plates are transformed into a two-dimensional spectral frame representation via Short Time Fourier Transform (STFT). The main idea of STFT is to

divide the longer time signal into short segments, and then compute the Fourier transform on each segment. Figure 5 shows the pre-process of transforming structural vibration into vibration spectrograms, which is explained in the following steps:

1. To capture the time and frequency domain information of the signal, a sliding window of 512 data points is selected that is moved from left to right each time step (0.0001 sec), and Fast Fourier Transform (FFT) is computed for each sliding window.
2. The sliding window of 512 data points moved over each time step (0.0001 sec) and the corresponding FFT result in a matrix of size 512×256 for each transient history.
3. The matrix of each transient history is transformed into a spectrogram, and each spectrogram is split half in width, and then supplied to CNN as a two-dimensional array of size 256×256×2.

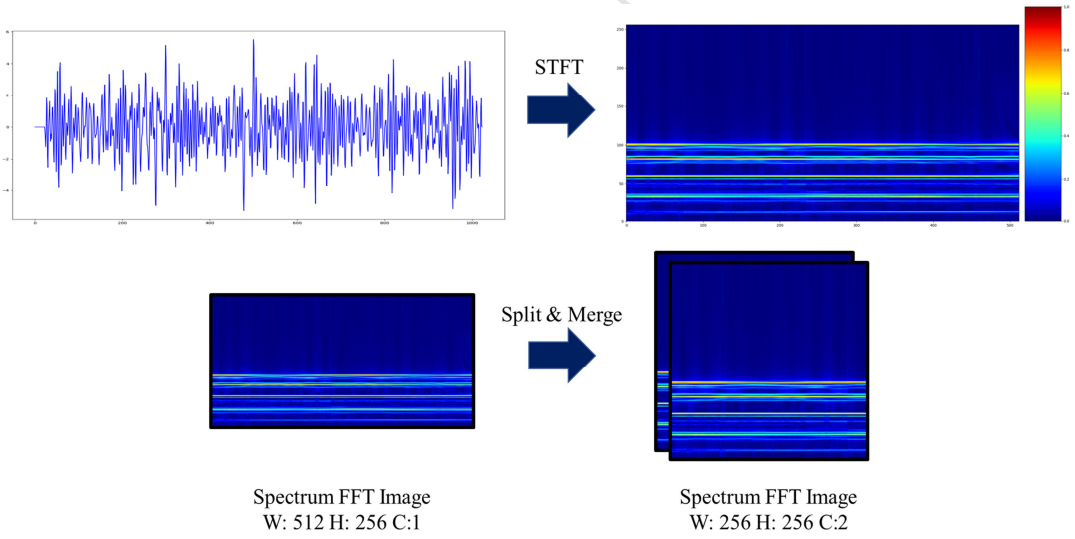

Figure 5. The pre-process of transforming transient responses into vibration spectrograms via STFT.

The process of transforming the transient histories of the healthy and delaminated cases into vibration-based spectrograms via STFT resulted in a total of 13,000 images that corresponded to 13 cases to be classified via CNN. In the next section, the architecture of CNN is developed to autonomously extract discriminative features from the vibration-based spectrograms, and employ those features to classify the healthy and delaminated cases into different classes.

4.3 CNN Architecture

This section discusses the architecture of CNN. Figure 6 shows that the network consists of six convolutional and pooling layers for automatically extracting discriminative features from the vibration-based spectrograms of the healthy and delaminated cases. Fully connected layer and Softmax layer is used to classify the healthy and delaminated cases on the basis of features extracted in the convolutional and pooling layers. Table 2 summarizes the detailed architecture of the proposed network.

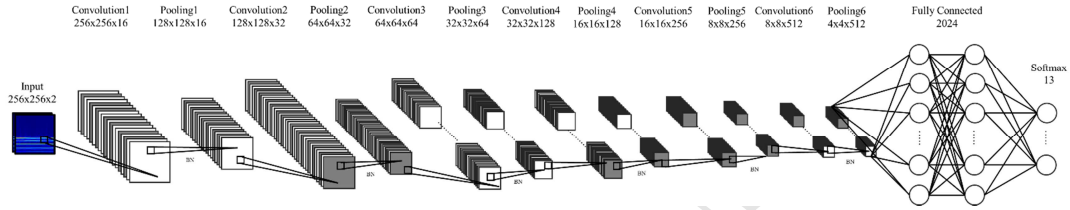

Figure 6. Proposed architecture of the network.

Table 2. Proposed Network Configuration.

Layer Name	Layer Description
Input	256×256 2-channel FFT Spectrum Image
Convolution 1, Pooling 1	Convolution Filter 3×3, strides 1, Number of filter = 16, ReLU, Batch normalization, Max Pooling Filter 2×2, strides 2
Convolution 2, Pooling 2	Convolution Filter 3×3, strides 1, Number of filter = 32, ReLU, Batch normalization, Max Pooling Filter 2×2, strides 2
Convolution 3, Pooling 3	Convolution Filter 3×3, strides 1, Number of filter = 64, ReLU, Batch normalization, Max Pooling Filter 2×2, strides 2
Convolution 4, Pooling 4	Convolution Filter 3×3, strides 1, Number of filter = 128, ReLU, Batch normalization, Max Pooling Filter 2×2, strides 2
Convolution 5, Pooling 5	Convolution Filter 3×3, strides 1, Number of filter = 256, ReLU, Batch normalization, Max Pooling Filter 2×2, strides 2
Convolution 6, Pooling 6	Convolution Filter 3×3, strides 1, Number of filter = 512, ReLU, Batch normalization, Max Pooling Filter 2×2, strides 2
Fully Connected	Input = 8,192, Output =2,024, ReLU

Softmax	Input = 2,024, Output =13

We initialize the weights randomly, and train all network weights from scratch. We use an Adam optimizer for fast calculation, and the models are trained with a mini-batch size of 13 on four TitanX GPUs. The learning rate is 0.0001, and the final models are trained for up to 200 epochs. To evaluate the proposed method, we basically used the repeated random subsampling validation protocol [44] with the data sets. We train and evaluate CNNs using ten-fold cross-validation at the proposed network architectures.

4.4 Classification of Delamination

The CNN architecture of section 4.3 was employed to classify the vibration-based spectrograms of the 13 classes (i.e., healthy and 12 delaminated cases). From the data set of 13,000 spectrograms, 11,700 spectrograms were used for training the network, while the remaining 1,300 were used for testing the network. CNN showed an overall classification accuracy of 90.1 % on the data set of 13,000 spectrograms. Although CNN showed a 10 % loss of classification accuracy, the results of the classifier are consistent with the physics of the problem, as seen from the confusion matrix of Fig. 7.

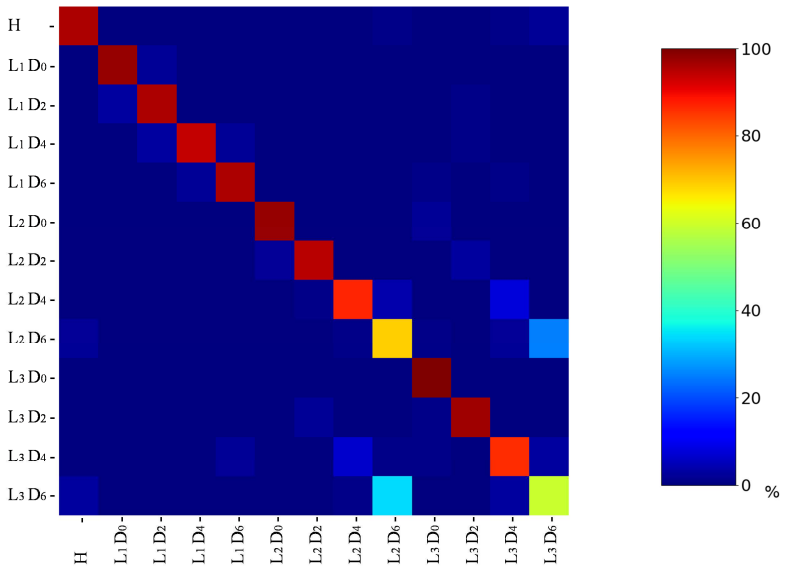

Figure 7. Confusion matrix of CNN in the classification of delamination.

Herein, the vertical axis shows the actual or true labels, while the horizontal axis shows the labels assigned by the CNN classifier to the healthy and delaminated cases. Figure 7 shows that the healthy case and the most severe cases of delamination: L1D0, L1D2, L1D4, L2D0, L2D2, L3D0, and L3D2 are correctly classified with a classification accuracy of more than 90 %. Specifically, 4 % instances of the healthy case are misclassified, out of which 2 % are misclassified as L3D6, 1 % are misclassified as L2D6, and 1 % are misclassified as L2D4. However, the misclassification results are consistent with the physics of the problem, because L3D6, L2D6, and L2D4 are the least severe cases of delamination, and may have the same response characteristics as the healthy case for certain loading conditions. Similarly, 3 % instances of the L1D2 are misclassified as L1D0, where the two have the same location along the length of the plate, and occur at such interfaces along the thickness that are nearer to each other (Fig. 2), hence the two may have the same response to certain loading conditions. The major loss of accuracy is mainly due to L2D6 and L3D6, where 25 % instances of L2D6 are misclassified as L3D6, and 34 % instances of L3D6 are misclassified as L2D6. However, the misclassification results are justifiable from the fact that delamination that occurs away from the fixed end in the lengthwise direction and near the free surface in the thickness direction is less severe in terms of loss of structural integrity, and is not easily detectable [31]. Hence the delamination cases of L2D6 and L3D6 are the least severe cases of delamination, and may have the same dynamic characteristics in terms of the sensed response that causes the CNN classifier to confuse these two cases of L2D6 and L3D6 with each other. Furthermore, the high classification accuracy of the least severe case at location L1 (i.e., L1D6) may be due to its proximity to the position of the sensor.

4.5 Testing on unseen cases of delamination

In this section, the pre-trained CNN classifier of section 4.4 is employed to predict labels for unseen cases of delamination. Herein, the term ‘unseen’ refers to the cases of delamination that have not been used in the training, cross-validation, and testing of the CNN classifier in section 4.4. Figure 8 shows a schematic of the so-called ‘unseen’ cases of delaminations: L1D1, L2D3, and L3D5:

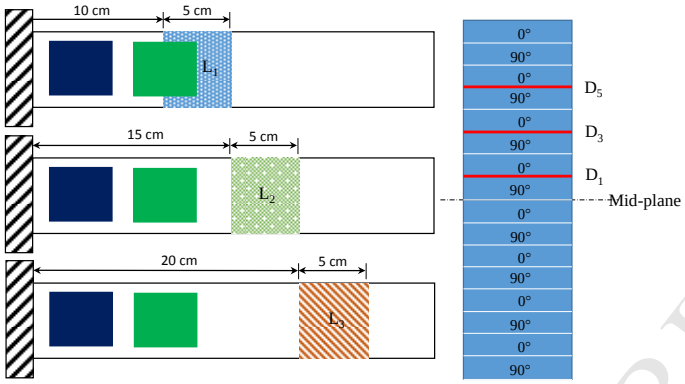

Figure 8. Schematic of the unseen cases of delaminations for testing the pre-trained CNN.

Figure 8 shows that the unseen cases of delaminations (i.e., L1D1, L2D3, and L3D5) are different from the delamination cases that have been used in the pre-trained CNN classifier regarding the through-thickness interfaces. For example, L1D1 occurs between L1D0 and L1D2 of the pre-trained network; similarly, L2D3 happen to be between L2D2 and L2D4, and so on. There are 10 instances in each case of the unseen delaminations that correspond to 10 random loadings. Table 3 shows the details of labels that are predicted by the pre-trained CNN for the unseen cases of delamination.

Table 3. Details of labels predicted by learned CNN for unseen cases of delamination.

Unseen Case L1D0										
Loading Number	1	2	3	4	5	6	7	8	9	10
Ground Truth Label	L_1D_1	L_1D_1	L_1D_1	L_1D_1	L_1D_1	L_1D_1	L_1D_1	L_1D_1	L_1D_1	L_1D_1
Labels predicted by Learned CNN	L_1D_0	L_1D_0	L_1D_0	L_1D_0	L_1D_0	L_1D_0	L_1D_0	L_1D_0	L_1D_0	L_1D_0
Unseen Case L2D3										
Loading Number	1	2	3	4	5	6	7	8	9	10
Ground Truth Label	L_2D_3	L_2D_3	L_2D_3	L_2D_3	L_2D_3	L_2D_3	L_2D_3	L_2D_3	L_2D_3	L_2D_3
Labels predicted by Learned CNN	L_2D_2	L_2D_2	L_2D_2	L_2D_2	L_2D_2	L_2D_2	L_2D_2	L_2D_2	L_2D_2	L_2D_2
Unseen Case L3D5										
Loading Number	1	2	3	4	5	6	7	8	9	10
Ground Truth Label	L_3D_5	L_3D_5	L_3D_5	L_3D_5	L_3D_5	L_3D_5	L_3D_5	L_3D_5	L_3D_5	L_3D_5
Labels predicted by Learned CNN	L_3D_4	L_3D_4	L_3D_4	L_3D_4	L_3D_4	L_3D_4	L_3D_4	L_3D_4	L_3D_4	L_3D_4

Table 3 reveals that the labels predicted by the learned CNN are consistent with the physics of the problem. For example, the dynamic characteristics of the L1D1 delaminated case should be similar to either the L1D0 or L1D2

delaminated case; the predicted label is L1D0, which shows the ability of the learned network to correctly predict those cases of delamination that were not even considered in the training and cross-validation of the network. The predictive performance of CNN in Table 3 shows that the proposed approach is able to correlate the occurrence of delamination and the corresponding loss of structural properties (e.g., structural stiffness) with the exact location and size of delamination, while only using low-frequency vibration outputs of a single sensor.

Although in the current work, deep learning neural network has been used for the assessment of delamination in smart composite laminates, the proposed approach could be extended to assess other types of damages (e.g., matrix crack, fiber failure, fiber-matrix debond, partial debonding of smart elements etc.) in laminated composites owing to the following assertions:

1. Different modes of failure cause the dynamic response signal to alter in different fashion
2. Deep learning neural network automatically extracts discriminative features from the dynamic response signals

Conclusion

Laminated composites are susceptible to various complex modes of failure, such as delamination. Although structural vibration responses obtained via smart elements, such as piezoelectric sensor, are readily available to assess laminated composites for the presence, localization and quantification of delamination, in the published literature, the attributes of low-frequency structural vibrations have been used for global assessment (i.e., the presence of damage), while features from high-frequency outputs (e.g., guided waves) have been employed for the local assessment (i.e., localization of damage) of smart composite laminates. In this paper, a method based on convolutional neural network (CNN) is proposed for the global and local assessment of delamination in smart composite laminates while using only low-frequency structural vibration outputs. An electromechanically coupled mathematical model is developed for the healthy and delaminated smart composite laminates by incorporating improved layerwise theory, higher-order electric potential field, and finite element method. Random structural vibration signals are obtained for the healthy and delaminated smart composites via a piezoelectric sensor, and Short Time Fourier Transform (STFT) is employed to transform those signals into 2-dimensional spectrograms. CNN is employed to automatically extract discriminative features from the vibration-based spectrograms, and employ those features to make a distinction between the healthy and delaminated scenarios, as well between various different scenarios of delamination. CNN showed an overall classification accuracy of 90.1 %, and the study of its confusion

matrix revealed that misclassification results are consistent with the physics of the problem. Furthermore, the pre-trained CNN classifier was employed to predict labels for the unseen cases of delamination, and physically consistent results were obtained. The obtained results show that the proposed approach may be employed for the detection, localization, and prediction of delamination in smart composite laminates using their structural vibration output only. Furthermore, the proposed approach does not require the time-consuming process of discriminative features selection that often requires human expertise, and in general, the selected features cannot be used for other configurations of the system.

Acknowledgement

This work was supported by the Basic Science Research Program through the National Research Foundation of Korea (NRF-2017R1D1A1B03028368), funded by the Ministry of Education.

References

[1] Chung DD. Composite materials: science and applications: Springer Science & Business Media; 2010.

[2] Elmarakbi A. Advanced composite materials for automotive applications: Structural integrity and crashworthiness: John Wiley & Sons; 2013.

[3] Gay D, Hoa SV, Tsai SW. Composite materials: design and applications: CRC press; 2002.

[4] Mouritz A, Gellert E, Burchill P, Challis K. Review of advanced composite structures for naval ships and submarines. Composite structures. 2001;53(1):21-42.

[5] Chróścielewski J, Miśkiewicz M, Pyrzowski Ł, Sobczyk B, Wilde K. A novel sandwich footbridge-Practical application of laminated composites in bridge design and in situ measurements of static response. Composites Part B: Engineering. 2017;126:153-61.

[6] Balakrishnan VS, Seidlitz H. Potential repair techniques for automotive composites: A review. Composites Part B: Engineering. 2018.

[7] Azouaoui K, Azari Z, Pluvinage G. Evaluation of impact fatigue damage in glass/epoxy composite laminate. International Journal of Fatigue. 2010;32(2):443-52.

[8] Heslehurst RB. Defects and damage in composite materials and structures: CRC Press; 2014.